

Modern Physics Letters B
 © World Scientific Publishing Company

Quantum phases of the frustrated XY models on the honeycomb lattice

Zhenyue Zhu

*Department of Physics and Astronomy, University of California, Irvine
 Irvine, CA 92617, USA
 zhenyuez@uci.edu*

Steven R. White

*Department of Physics and Astronomy, University of California, Irvine
 Irvine, CA 92617, USA
 srw@uci.edu*

Received (22 October 2014)

Accepted (3 November 2014)

Searching for spin liquid states has long been attracting both experimentalists and theorists. In this article, we review recent density matrix renormalization group studies of the spin-1/2 XY model on the honeycomb lattice, with first-neighbor ($J_1 = 1$) and frustrating second-neighbor ($J_2 > 0$) interactions. For the intermediate frustration regime $0.22 \lesssim J_2 \lesssim 0.36$, there exists a surprising antiferromagnetic Ising phase, with ordered moments pointing along the z axis, despite the absence of any $S_z S_z$ interactions in the Hamiltonian. Surrounding this phase as a function of J_2 are antiferromagnetic phases with the moments pointing in the x - y plane for small J_2 and a close competition between an x - y plane magnetic collinear phase and a dimer phase for large values of J_2 . No spin-liquid phases was found in the XY model even with the third neighbor ($J_3 > 0$) interactions.

Keywords: frustration; XY model; spin liquid; honeycomb lattice; DMRG.

1. Introduction

Progress in finding model quantum Hamiltonians with spin-liquid (SL) ground states has accelerated dramatically in the last two years, almost 40 years since Anderson first proposed a resonating valence bond (RVB) state as a possible ground state of the triangular Heisenberg model.¹ However, it was later shown that the ground state has antiferromagnetic $\sqrt{3} \times \sqrt{3}$ order, where the moments lie in the same plane with 120° angles between neighboring spins.²

The main defining feature of a quantum spin liquid is the absence of any spontaneously broken symmetry, particularly either magnetic or valence-bond order. Frustration, which discourages order, is a key ingredient of models potentially containing spin liquid phases. Spin liquids arise in several analytic treatments and exactly solvable, simplified, but less realistic models.³ A key feature distinguishing types of spin liquids is the presence or absence of a gap to all excitations. To

satisfy the Lieb-Schultz-Mattis theorem, gapped spin liquids for models with a net half-integer spin per unit cell must have “hidden” topological degeneracies in the thermodynamic limit, which depending on the topology of the system. These topological SL states possess “hidden” non-local order — long range entanglement. The simplest possibility is a Z_2 spin liquid. There are two classes of lattice models with hard local constraints, namely the quantum dimer^{4,5} and loop models (toric code⁶ and string-net model⁷) that possess Z_2 topological SL ground state.

The quantum dimer model was first introduced by Rokhsar and Kivelson⁴ on the square lattice, where the degrees of freedom consist of dimers on links with a constraint that there is only one dimer touching each vertex. At the RK point, the ground state is the equal weight superposition of all possible dimer coverings on the square lattice (RVB state). It was later generalized by Moessner and Sondhi⁵ to the triangular lattice, where the system has a Z_2 topological ground state. There are four degenerate ground states on a torus, since there are two non-contractible loops; each loop can possess even or odd parity, depend on whether a loop cuts an even or odd number of bonds. Note that on a small finite size torus, these states are not degenerate, with an energy splitting between different topological sectors decaying exponentially with the loop size. The toric code model also has Z_2 topological order with 4 fold ground state degeneracy on a torus.

Since local measurements cannot identify Z_2 or other topological order, it is challenging to identify its presence in a numerical study. The degeneracies characteristic of a 2D gapped Z_2 spin liquid have not been accessible for the system sizes studied to date. Odd-width cylinders spontaneously dimerize in a pattern that is characteristic of a quasi-one-dimensional system.⁸ Besides these properties for a Z_2 topological SL state, another key feature of a Z_2 spin liquid is the presence of topological entanglement entropy (TEE) γ introduced by Kitaev-Preskill⁹ and Levin-Wen¹⁰. For a topological phase, $\gamma = -\ln D$, where D is the total quantum dimension of the system. For conventionally ordered phases, $D=1$. For topological states, $D > 1$. Physically we can understand the origin of this term using the toric code or string net model. These models have a wavefunction describing closed loops. Each loop must cross the boundary twice, thus there is a reduction of entanglement entropy. For a Z_2 topological state $\gamma = -\ln 2$.

The quantum dimer and toric code models are artificial Hamiltonians constructed with a delicate topological order. The last few years have seen a major resurgence in both experimental and theoretical interest in quantum spin liquid ground states. Much of the interest stems from strong evidence that quantum spin liquids exist experimentally in several different materials.³ In the case of the kagome lattice material Herbertsmithite $\text{ZnCu}_3(\text{OH})_6\text{Cl}_2$ with all the Cu^{2+} carrying spins $S=1/2$ occupy the sites of a Kagome lattice in weakly coupled layers, there are substantial experimental evidence that this material has a spin liquid low temperature phase, with no magnetic or valence bond order down to 50mk, along with a gapless spin excitations.^{11,12,13,14,15} The effective Hamiltonian can be described by the spin $S=1/2$ Heisenberg Kagome anti-ferromagnetic model.

This SL state has coincided with recent strong numerical evidence that the spin-1/2 Heisenberg kagome antiferromagnet has a spin liquid ground state,⁸ and that this state has Z_2 topological order,¹⁶ since a $-\ln 2$ constant term correction to the linear growth of the entanglement entropy with subsystem perimeter is observed. The same thing happens for the kagome system with next-nearest-neighbor interaction J_2 ,¹⁷ where for $J_2 = 0.1$ the gaps are large and the entanglement entropy correction term can be measured particularly precisely. Thus, there is now solid evidence that the ground state of the kagome spin-1/2 antiferromagnet is a gapped Z_2 spin liquid. However, the most important issue is that Herbertsmithite seems to be a gapless SL, where the Z_2 SL state is fully gapped. Hopefully this discrepancy can be solved by refining the model Hamiltonian for the real material. So there is great interest in understanding the kagome SL in more detail, and in finding other SLs in simple realistic models.

The numerical work has become possible through continued advances in density matrix renormalization group (DMRG) techniques;^{18,19,20} these methods can now be used to study frustrated spin Hamiltonians on cylinders with widths up to 12 or 14 lattice spacings, which, when combined with careful finite size analysis, can determine phases and properties in the two-dimensional thermodynamic limit with good confidence in many cases. At the same time, the reduced density matrix is calculated in the DMRG algorithm at each sweeping step. Therefore we can directly compute the entanglement entropy from DMRG.

SL phases have been suggested for various other realistic models, such as the half-filled honeycomb Fermi-Hubbard model²¹ and the square lattice spin-1/2 Heisenberg antiferromagnet with second-neighbor (J_2) interactions.^{22,23} However, some skepticism has been expressed about the evidence for spin liquids in these two models.^{24,25} There are two very recent papers pointing out that these two models do not possess SL ground states. The half-filled honeycomb Fermi-Hubbard model only has one single phase transition at $\frac{U}{t} \sim 3.78$ between a semi-metal phase for small U and an AFM state for large U .²⁶ A recent DMRG calculation carefully analyzed the $J_1 - J_2$ model on the square lattice and showed that there is a much stronger square plaquette valence bond pattern for intermediate coupling at $0.5 < J_2 < 0.6$, showing that the plaquette correlation length increases faster as the cylinder gets wider.²⁷

In 2011, Varney *et al.*²⁸ studied the spin-1/2 XY model on the honeycomb lattice, with first-neighbor ($J_1 = 1, \langle i, j \rangle$) and frustrating second-neighbor ($J_2 > 0, \langle\langle i, j \rangle\rangle$) XY interactions, with Hamiltonian

$$H = J_1 \sum_{\langle i, j \rangle} (S_i^+ S_j^- + H.c.) + J_2 \sum_{\langle\langle i, j \rangle\rangle} (S_i^+ S_j^- + H.c.). \quad (1)$$

Based on exact diagonalization (ED) of various small clusters, they suggested that a particular spin-liquid ground state, a “Bose liquid,” appears for $0.21 \lesssim J_2 \lesssim 0.36$. Bose liquids may have a singular surface in momentum space, similar to a Fermi surface for a Fermi system, with gapless excitations and power-law correlations,^{29,30}

or they may be gapped and incompressible.^{31,32} This spin model is equivalent to spinless hard-core bosons with first- and second-neighbor hopping and zero off-site interactions.

Later on, DMRG calculations on large cylinders showed that although the locations of the two phase boundaries and the properties of the phase for small J_2 are correct, the intermediate phase has long-range Ising antiferromagnetic order, instead of the Bose metal phase.³³ This phase was not noticed in previous work on smaller systems. In terms of bosons, this intermediate Ising phase has “charge-density” order of the bosons, with higher density on one sub-lattice than the other. Afterwards, the coupled cluster method also verified the existence of this Ising ordered phase.³⁷

In the rest of the paper, we will review the progress of the $J_1 - J_2$ XY model on the honeycomb lattice, and also present some new results unpublished before. In Sec. 2, we present the results of DMRG calculations on this model, including the determination of the phase transition points, properties of the Ising antiferromagnetic order at $J_2 = 0.3$, and the competition of the dimer and collinear state at large J_2 . In Sec. 3, we include the further neighbor interaction J_3 in the Hamiltonian to study the phase diagram on the XC8 cylinder. In Sec. 4, we study the transition between $J_1 - J_2$ XY and Heisenberg model at $J_2 = 0.3$. We summarize the results in Sec. 5.

2. Quantum phases of the $J_1 - J_2$ XY model

In this section, we review the results obtained using DMRG on the $J_1 - J_2$ XY model on the honeycomb lattice and compare the results with other numerical techniques, such as series expansions and the coupled cluster method. In the unfrustrated limit $J_2 = 0$, the ground state has the expected Néel order in the xy plane. We find that this phase extends to $J_2 \sim 0.22$. In the interval $0.22 \lesssim J_2 \lesssim 0.36$, we find an antiferromagnetic phase that surprisingly has staggered magnetization polarized along the z -direction in spin space; we call this Ising antiferromagnetic order, to distinguish it from Neel order in the xy plane. Finally, for $J_2 \gtrsim 0.36$, we find that there is a close competition between a magnetically ordered xy -plane collinear phase and a magnetically disordered dimer phase.

2.1. Setup of cylinder geometries for the DMRG calculation

We have performed numerous DMRG^{18,19,20} calculations on this model on long cylinders with circumferences up to 12 lattice spacings. The properties of the ground state are governed by the ratio J_2/J_1 . In all of our calculations, we take $J_1 = 1$ and $0 \leq J_2 \leq 1$, thus antiferromagnetic interactions. The cylinder geometries we used in our DMRG calculations are adopted from Ref. 34. For example, XC8 represents a cylinder where one set of edges of each hexagon lie along the x direction (which always coincides with the cylinder axis), and there are 8 spins along the circumferential zigzag columns, connected periodically (Fig. 1(a)). The actual circumference

(Euclidean distance) of XC8 is $C = 4\sqrt{3}$ lattice spacings. For the YC6 cylinder, one set of edges of each hexagon lies along the y (circumferential) direction and there are 6 spins (in 3 pairs) along a straight circumference of $C = 9$ lattice spacings [Fig. 6(b)]. For narrow cylinders like XC8, we are easily able to achieve a truncation error of about 10^{-8} with $M = 2400$ states, which determines the ground state essentially exactly. For YC8, our widest cylinder with $C = 12$, we need to keep $M = 5800$ to achieve a truncation error of 10^{-6} —still excellent accuracy. In all our DMRG calculations, we keep enough states to make sure that the truncation error is smaller than 10^{-6} .

When performing DMRG calculations on cylinders, we have to map the lattice into a one dimensional chain and start the regular sweeping process. Let A and B denote two different sub-lattice on the honeycomb lattice. In the XC cylinders, we find that it is better to map into the 1D vertical zigzag chains one by one (AB site chains), instead of all the straight columns of sites (A site chain, B site chain). Otherwise, it is easy to get stuck in a higher energy state on wider cylinders which have magnetic domain walls.

2.2. Determination of the phase transitions

The classical phase diagram of the $J_1 - J_2$ XY model on the honeycomb lattice has the following phase diagram: for $0 < J_2 < \frac{1}{6}$, it is the Neel order with wave vector Q located at the center of the Brillouin zone (Γ point); For $\frac{1}{6} < J_2 < \frac{1}{2}$, it is the coplanar spiral I phase with Q forms closed contours around the Γ point; At $J_2 = \frac{1}{2}$, it is the collinear state with nearest neighbor bonds are ferromagnetic in one direction and antiferromagnetic in the other two direction with the closed contour has a hexagonal shape and touch the edge center of the Brillouin zone (M point); For $J_2 > \frac{1}{2}$, it is the spiral II phase with closed contours around the corner of the Brillouin zone (K or K' point).³⁵ Considering quantum correlations to the classical spin waves, it is found that the Neel state extends up to $J_2 = 0.26$, well beyond the classical value $\frac{1}{6}$. On the other hand, the collinear state is stable from $J_2 = \frac{1}{2}$ to a regime of $0.26 < J_2 < 1$.³⁵ In the quantum limit of the phase diagram, the critical point usually expands to an intermediate phase. Therefore, we would expect that there will be a intermediate phase between Neel order and collinear order state. Next we will apply DMRG to investigate the quantum phase diagram.

In Fig. 1, we present two cylinders to first give a quick summary of the whole phase diagram. These are XC8 cylinders in which J_2 is varied along the length of the cylinder, showing locally the various phases. In Fig. 1(a), J_2 varies from 0.12 to 0.30. At the $J_2 = 0.12$ left edge, a staggered field in the xy plane was applied to “pin” the Neel order. The ordered moments rotate from the x to the z direction, indicating that there is a phase transition between Neel and Ising order, at $J_2 \sim 0.22$. In Fig. 1(b), J_2 is varied from 0.28 to 0.46, with AF pinning fields along the x direction at the $J_2 = 0.46$ right end to show the collinear pattern. The phase transition from

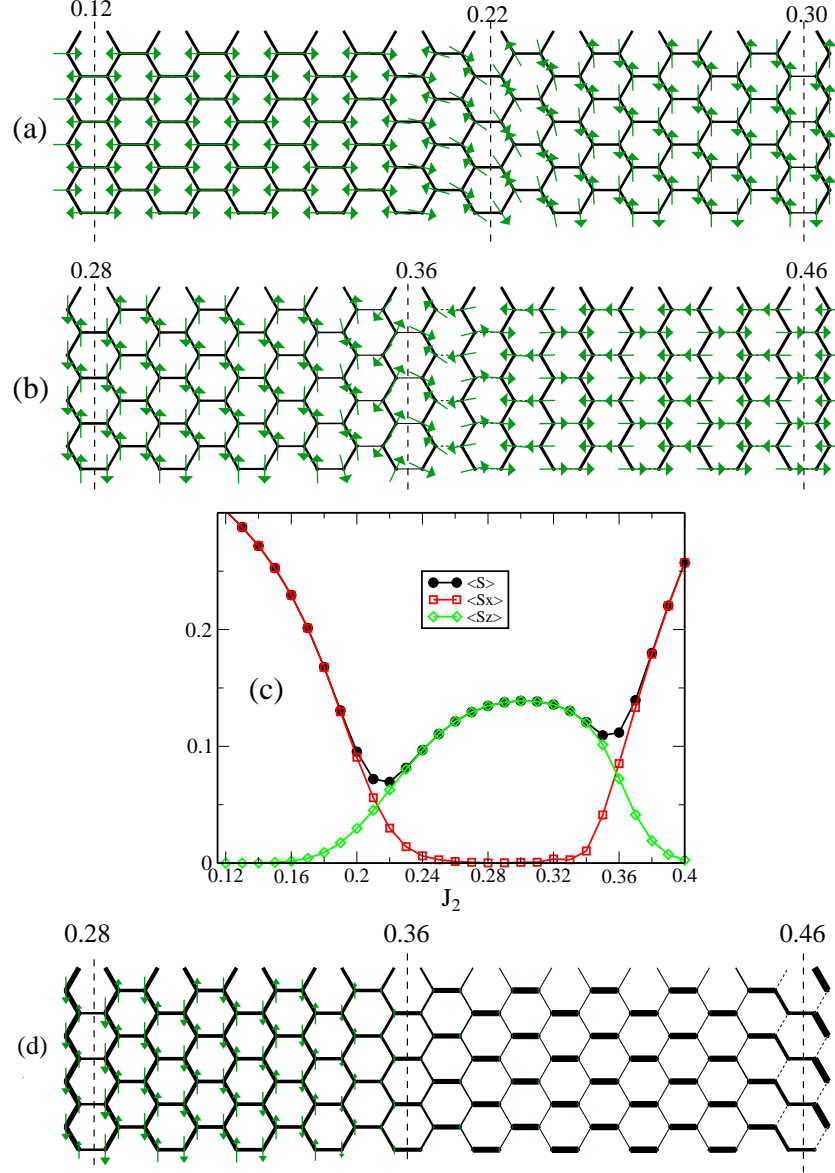
6 *Zhenyue Zhu and Steven R. White*

Fig. 1. (a) Local magnetic moments along the XC8-0 cylinder with J_2 varying along the length of the cylinder. The length of the arrows are fixed, while their angle correctly represents the spin orientation. The dashed lines show particular J_2 s, which are constant along a column of hexagons. In (a), we show a system with J_2 varying from 0.12 to 0.30. For $J_2 \sim 0.22$, the xy-plane Neel order flips to z-direction Ising order. In (b), J_2 is varied from 0.28 to 0.46. The second phase transition point is located at $J_2 \sim 0.36$ between Ising and metastable collinear state. (c) shows the size of $|\langle S \rangle|$, $|\langle S_x \rangle|$, $|\langle S_z \rangle|$ along the cylinder column versus J_2 . The phase transition is apparent at J_2 s where $|\langle S \rangle|$ is a minimum. (d) shows the phase transition from Ising order to dimer order with phase transition point is also located at $J_2 \sim 0.36$.

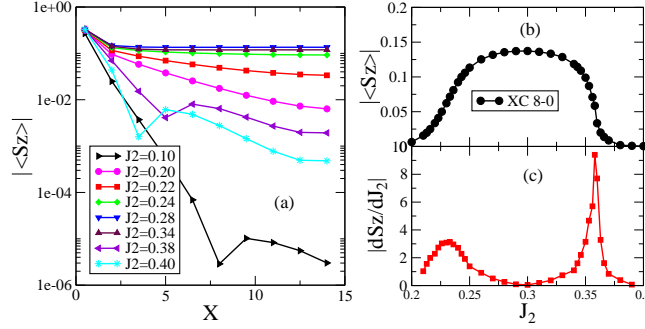


Fig. 2. (a) Local magnetization $|\langle S_z \rangle|$ versus distance from the end of an XC8 cylinder for various J_2 values. (b) The magnetization at the cylinder center versus J_2 . (c) The derivative of the central $|\langle S_z \rangle|$ versus J_2 . The peaks of the derivative at $J_2 = 0.23$ and 0.36 indicate the two phase transition points. From Zhu *et al.* Ref. 33.

Ising to metastable collinear order is visible at $J_2 \sim 0.36$, where spin flips to x direction again. In Fig. 1(c), we show the actual size of $|\langle S \rangle|$, $|\langle S_x \rangle|$, $|\langle S_z \rangle|$ for each J_2 . It's clearly seen that the intermediate phase has $|\langle S_z \rangle| \sim 0.14$ with $|\langle S_x \rangle| = 0$. The minimum of $|\langle S \rangle|$ locates the two phase transition points at $J_2 = 0.22$ and 0.36 . We also show in Fig. 1(d) that the phase transition between Ising order and dimer order is also located at $J_2 = 0.36$, since ground state in the XC8-0 cylinder at large J_2 is the a dimer instead of collinear state. See next section for the detailed discussion of the collinear and dimer states. We also applied these methods to other cylinders and find that the values of J_2 at the estimated phase transitions change only slightly between different width and orientation cylinders. Thus the locations of these phase transitions show only small finite size effects, which is consistent with our agreement with the small-size ED results from Ref. 28.

In Fig. 2, we apply a staggered field with $h_z = 0.5$ at a cylinder end to measure the decay of $|\langle S_z \rangle|$ with distance from the end for various values of J_2 . As shown in Fig. 2(a), $|\langle S_z \rangle|$ decays exponentially within both the Neel and the dimer phases, but the correlation length gets longer and $|\langle S_z \rangle|$ becomes spatially uniform in the cylinder center for the Ising ordered phase. In Fig. 2(b), we show the magnetization in the cylinder center versus J_2 . It is clear from this plot that the intermediate Ising phase is a broad regime, and from its derivative versus J_2 , we determine the two phase transition points at ~ 0.23 and 0.36 , which approximately match the phase transitions determined from Fig. 1. It is interesting to note that $|\langle S_z \rangle|$ is almost independent of J_2 for much of this intermediate Ising phase. The moment $|\langle S_z \rangle| \sim 0.14$ is strongly reduced from the maximum “classical” value of 0.5 .

The derivative of $|\langle S_z \rangle|$ shown in Fig. 2(c) shows markedly different behavior for the two transitions, with the second transition being much sharper. A natural interpretation is that the phase transition between Neel and Ising phases is continuous, but the second phase transition point is first order. To test this, we have

performed calculations on cylinders with a much narrower range of J_2 values along the length of the cylinder, zooming in on the transitions. If the phase transition is first order, we expect that the phase transition region should remain narrow as we zoom in. For a continuous phase transition, the phase transition region should broaden as we zoom in. Varying the gradient of J_2 by a factor of 5, we do find that the Neel-Ising phase transition region broadens, but the second phase transition region stays narrow. Thus, it does appear that the former is continuous, and the latter is first order. However, any conclusions about the second transition are tentative, because of the close competition between the dimer and collinear phases for $J_2 > 0.36$.

In comparison, the fidelity measurement from the exact diagonalization on small size clusters found two phase transition points at 0.210(8) and 0.356(9).²⁸ Series expansions, measuring the local magnetization in the Neel and collinear phases, determined phase transitions at 0.22(1) and around 0.35.³⁶ Similarly, the coupled cluster method determined the two phase transition points at 0.216(5) and 0.355(5).³⁷ Therefore, it is believed that the two phase transition points are located around 0.22 and 0.36 in the thermodynamic limit with an intermediate phase between them.

2.3. *The detailed study of ground state properties at $J_2 = 0.3$*

We have tested the stability of the Ising phase in several ways. For example, one can measure the decay of the local staggered magnetization away from an applied staggered field on an end of the cylinder. For the Neel ordered phase (small J_2), when we apply the pinning magnetic field along the z direction, $|\langle S_z \rangle|$ decays exponentially from the cylinder end [Fig. 3(a)]. To similarly test the Ising phase, we apply the pinning field along the x direction at the ends of an XC8 cylinder with $J_2 = 0.3$. We find that $|\langle S_x \rangle|$ decays exponentially with distance from the cylinder end with a very short correlation length $\xi_x = 1.8$, but $|\langle S_z \rangle|$ rises from the end and saturates in the center of cylinder (not shown). This provides solid evidence that Ising order is very robust on this cylinder. As another test, we have measured the correlation function $|\langle S_i^+(0) S_j^-(x) \rangle|$ and find that its correlation length decreases as a function of increasing J_2 for J_2 near 0.22, and then increases rapidly for J_2 near 0.36. The minimum correlation length is roughly $\xi \sim 1.5$ at $J_2 = 0.3$ (not shown). This result again confirms that xy -plane order is absent in the intermediate phase.

We also measured the entanglement entropy for various cylinder sizes and extrapolated to see if there is a possible topological entanglement entropy contribution (γ) in Fig. 4(b). Entanglement entropy area law states that for a gapped phase entanglement entropy only depends on the boundary size, independent of the subsystem size.

$$S \sim aL + \gamma + O(1/L), \quad (2)$$

with L its boundary length.³⁸ In Fig. 3, we show the entanglement entropy versus the subsystem size x for various XC and YC cylinders. For XC cylinders, the entropy

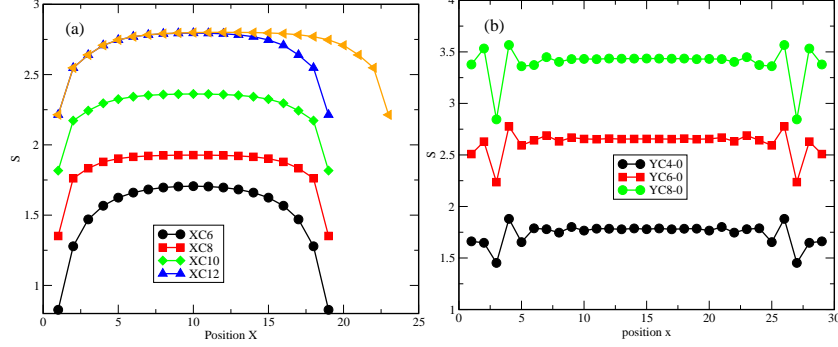


Fig. 3. The unextrapolated ground state entanglement entropy versus subsystem size x for (a) XC cylinders and (b) YC cylinders. The entanglement entropy for the widest cylinder shown here is not quite converged, where the number of states kept is $M=5600$.

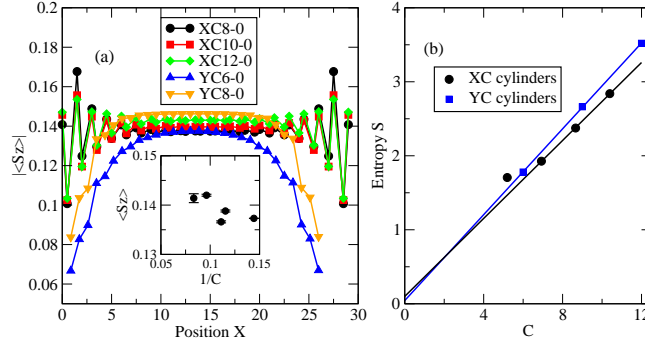


Fig. 4. (a) The absolute value of the local magnetization $|\langle S_z \rangle|$ for various XC and YC cylinders versus distance along the cylinder. The inset shows the extrapolated magnetization (extrapolated versus the truncation error) at the cylinder center, with error bars, versus the inverse of cylinder circumference C . (b) The entanglement entropy versus circumference for XC and YC cylinders in the intermediate Ising ordered phase at $J_2 = 0.3$. The intercepts are consistent with zero. From Zhu *et al.* Ref. 33.

is lower at the cylinder ends, but saturated in the cylinder center independent of the cylinder length. The entropy oscillates near the YC cylinder edges, because the system shows plaquette pattern only at the edges with short PVB correlation length.

We then use the entropy at the center for various cylinders (extracted from Fig. 3) to linear extrapolate γ from the above equation. For a Z_2 spin liquid, one would expect $\gamma = -\ln 2$. We find $\gamma \sim 0.09$ for XC cylinders and $\gamma \sim 0.04$ for YC cylinders, values consistent with zero, as expected for a non-topologically ordered state. We expect that if we could include larger cylinders, the resulting data would extrapolate to $\gamma = 0$.

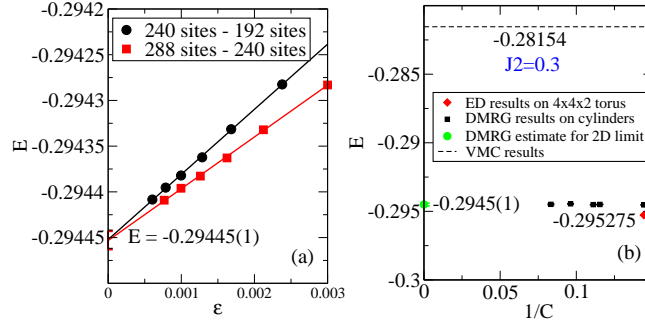


Fig. 5. (a) The extrapolation of the ground state energy per spin for $J_2 = 0.3$ versus truncation error for the XC12 cylinder. The black curve is the energy per spin from subtracting the energies of two XC12 cylinders with lengths $L_x = 20$ and $L_x = 16$. The red curve is from subtracting two cylinders with $L_x = 24$ and $L_x = 20$. These two subtractions extrapolate to the same energy per spin of $-0.29445(1)$. (b) The ground state energy per spin for $J_2 = 0.3$ versus the inverse of cylinder circumference from our DMRG calculations, compared with the variational Monte Carlo (VMC) result from Table III in the supplemental material, and exact diagonalization. From Zhu *et al.* Ref. 33.

To make sure that the Ising order is not a finite size effect, we have studied the $J_2 = 0.3$ system for cylinders with various widths. Figure 4(a) shows $|\langle S_z \rangle|$ as a function of x for XC and YC cylinders. In the inset, we plot the extrapolated magnetization at the cylinder center versus the inverse of the cylinder circumference. For these cylinders, the staggered magnetization is nearly constant with circumference, taking a value of about $0.135 - 0.142$. Thus, we believe that $|\langle S_z \rangle| \sim 0.14$ in the 2D limit for $J_2 = 0.3$. If anything, the staggered magnetization increases with increasing C , so this should be viewed as a lower bound on the value in the 2D limit.

We have not been able to find a simple analytical argument or calculation that gives an intuitive picture for this robust Ising ordered state. However, viewing the system as hard-core bosons at half filling provides an additional perspective. The Hamiltonian can be mapped straightforwardly and exactly into a hard-core boson model with first-neighbor hopping $t_1 = J_1/4$ and second-neighbor hopping $t_2 = J_2/4$, since $S^\dagger = b^\dagger/2$, $S^z = b^\dagger b - 0.5$. The Ising order would appear as a charge density wave (CDW) order, where the density is higher on sub-lattice A ($n_A \sim 0.64$) than on sub-lattice B ($n_B = 1 - n_A \sim 0.36$). Although there are only hopping terms in this hard-core boson Hamiltonian, the hard-core constraint (one boson per lattice site) is an on-site interaction. One could imagine that this on-site interaction renormalizes in some way to produce a first-neighbor density-density interaction, which could produce the CDW. This system is the first that we are aware of where a CDW is produced only from the combination of frustrated hopping and a hard-core constraint.

Very recently, a variational Monte Carlo study of this model has appeared.³⁹ In Ref. 39, a variational spin-liquid wave function is constructed by decomposing

the boson operators into a pair of fermions with a long-range Jastrow factor, with Gutzwiller projection enforcing single occupancy. At $J_2 = 0.3$, the lowest energy for such a state had energy per spin $E = -0.28154$, which is $\sim 4\%$ higher than ED of the $4 \times 4 \times 2$ torus ($E = -0.295275$)³⁹. Although this might appear to be a small difference in energy, for competing phases in geometrically frustrated spin-1/2 models near spin liquids, this is actually a very large energy difference. For example, the spin-1/2 kagome antiferromagnet (with $J_2 = 0$) has an energy difference of only about 1% between the (metastable) honeycomb valence bond crystal and the spin-liquid ground state.⁸ In our DMRG calculations, the energy per spin for a specific cylinder geometry can be calculated by subtracting two cylinders with the same width but different lengths.²⁰ When the cylinder is long enough, this method gives the energy per spin in the cylinder center, with minimal edge effects. We show in Fig. 5(a) that the energy per spin from subtracting two different pairs of cylinders gives precisely the same energy for the XC12 cylinder. Thus, we find that the ground state energy per spin is $-0.29445(1)$ for an infinitely long XC12 cylinder at $J_2 = 0.3$. In Fig. 5(b), we compare our DMRG results for the ground state energy on various cylinders at $J_2 = 0.3$. For the cylinders we study, the DMRG energies have quite small finite size effects. We estimate that the ground state energy is $E = -0.2945(1)$ in the 2D limit. The small-size ED result is only slightly ($\sim 0.26\%$) lower in energy, due to its finite size effects. The state DMRG finds has antiferromagnetic Ising order with the spin moments ordered in the z direction. This ordered ground state has much lower energy than the variational spin-liquid state.

At $J_2 = 0.3$, series expansions fail to give accurate ground states for the Ising phase due to poor convergence. However, indirect evidence to support the Ising antiferromagnetic order phase is that the $\langle S_x^i S_x^j + S_y^i S_y^j \rangle$ correlations decrease, while the $\langle S_z^i S_z^j \rangle$ correlations increase with J_2 and approach the same value near the first phase transition point at $J_2 = 0.22$.³⁶ It's expected that the $\langle S_z^i S_z^j \rangle$ correlations will dominate in the intermediate phase regime as in the z -direction Ising AF order. The coupled cluster method starts from the Ising ordered state as a reference state and finds a ground state energy $E = -0.2947$ and magnetization $M = 0.138$ in the 2D limit, very similar to the DMRG results.³⁷ It would be interesting to check these results with other numerical techniques in the future.

2.4. The competition between VBC and collinear order for large J_2

At large J_2 s, we find that both collinear and dimers state can be stabilized on even XC cylinders. We will start from the XC8-0 cylinders and discuss how we analyze this issue. When we perform DMRG calculations from different random states, we can produce different final states. For example, at $J_2 = 0.4$, we can easily get a collinear state (Fig. 6d) and (less likely) also get a dimer state (Fig. 6a). The opposite happens for $J_2 = 0.5$. Therefore it appears that both dimer and collinear states are stable on the XC8-0 cylinder. We add extra terms in the Hamiltonian to prepare different initial state and then remove these extra terms

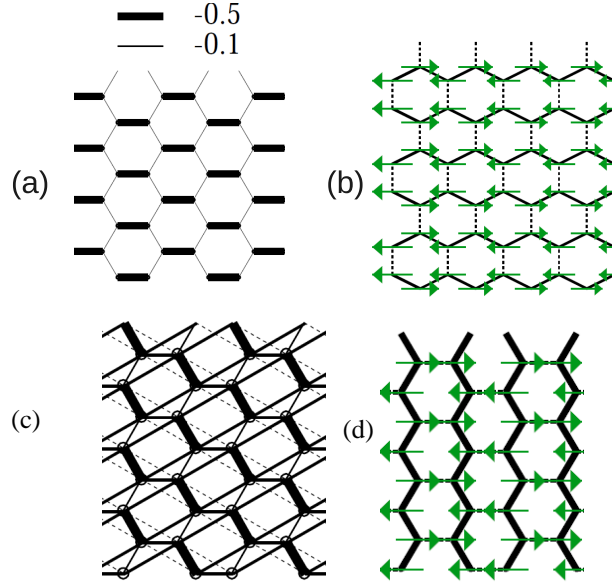


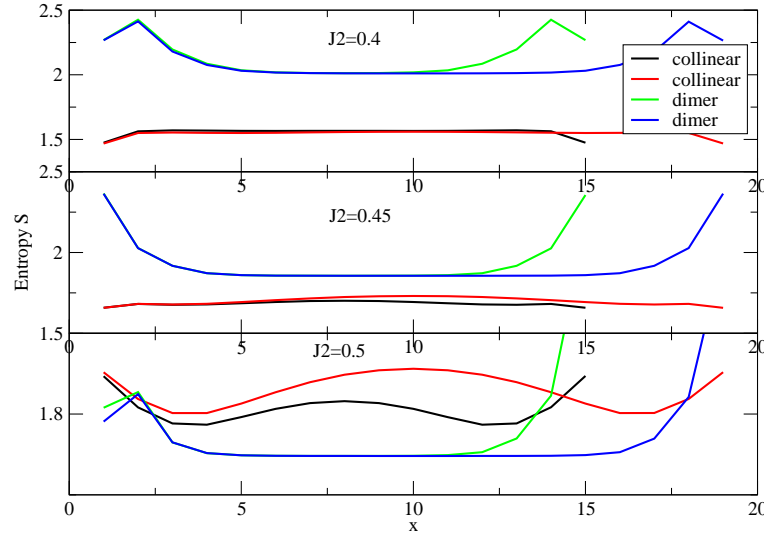
Fig. 6. (a) The ground state on the XC8 cylinder at $J_2 = 0.5$, showing strong dimer correlations aligned horizontally. We call this state a dimer state or SVBC. It has strong J_2 bonds connecting these dimers vertically and wrapping around the cylinder (not plotted in this figure). (b) The ground state on YC6 cylinder at $J_2 = 0.5$. It has xy -plane collinear magnetic order, with antiferromagnetic chains along the horizontal zigzag direction together with ferromagnetic first-neighbor correlations between these zigzag chains. (c) The ground state on XC8 cylinder at $J_2 = 0.37$ shows the diagonal SVBC with ladder pattern. (d) The metastable collinear state on the XC8-0 cylinder at $J_2 = 0.5$.

after several sweeps. For example, to start from a dimer state, we strengthen the horizontal bonds ($S_i^+ S_j^- + h.c.$) of the XC cylinder by 20%. For an initial collinear state, we weaken these bonds by 20% to enforce the strong bonds along the vertical zigzag direction. Since the collinear state has magnetic order along the xy plane, we can also apply the pinning field along the x direction on the cylinder edges and measure the S_x locally, which is possible by not keeping the quantum number S_z conserved. Starting from different possible collinear states on the XC8-0 cylinder, it turns out that only the collinear pattern shown in Fig. 6(d) is a stable collinear state. These results are presented in the following table. The second and fourth column are calculated with quantum number S_z conserved, while the third column is calculated without quantum number conservation, but with fields applied along the x direction on the cylinder edges to show the proper collinear magnetic pattern. The two different calculations for the collinear state have exactly the same energy, but the ground state for these cylinders are actually a dimer state.

We look at the entanglement entropy to understand these different states in Fig. 7. At $J_2 = 0.4$, the entanglement entropy for the collinear state is much lower than

Table 1. The energy for different states on the XC8-0 cylinder at various J_2 s.

J_2	collinear	edge h_x	dimer
0.40	-0.29815	-0.29814	-0.3007
0.45	-0.30778	-0.30778	-0.3112
0.50	-0.31896	-0.31895	-0.3229

Fig. 7. The entanglement entropy for collinear and dimer states at different J_2 s versus the position of the entanglement cut for the XC8-0 cylinders. There are two collinear and two dimer states with different length for each subfigure.

the dimer state. Since we know that the DMRG algorithm prefers the low entropy state if energies are nearly degenerate, DMRG could easily get the collinear state (low entropy but high energy state) from a random state at $J_2 = 0.4$, instead of the dimer state (high entropy but low energy state). At $J_2 = 0.5$, the dimer state actually has lower entropy than the collinear. Thus DMRG finds the correct ground state - a dimer state with low entropy and low energy. The entropy is measured from dimer and collinear states with quantum number S_z conserved. For the collinear state with edge fields applied along the x direction, the entropy is lower, since this state has only magnetic moments pointing in one specific direction, instead of a superposition of all possible directions in the xy plane.

The horizontal dimer state on the XC8-0 cylinder has strong J_2 bonds connecting them to form ladders wrapping periodically around the cylinder with length 4. Therefore the horizontal dimer state can only appear on even XC4N-0 cylinders with ladder length $2N$ to accommodate the AFM correlation. Thus we do not obtain stable horizontal dimer states on the XC10-0 cylinder. For the YC cylinders,

the possible dimer state should be vertical with J_2 bonds connecting them to form the ladders horizontally. However, we find that at $J_2 = 0.5$, vertical dimer states can not be stabilized in our DMRG calculation. Initially pinned dimer states always evolve to collinear states. The only stable dimer state on the YC cylinder is at small J_2 , say $J_2 = 0.4$. Another interesting thing about YC cylinders is that the collinear state pattern can have AFM correlation on the zigzag chains either along the horizontal direction (Fig. 6(b)) or wrapping around the cylinder with some angle (when we start from a random state). These two states have very similar energies. The results are presented in the following table for $J_2 = 0.40, 0.45$ and 0.50 .

Table 2. The energy for different states on various cylinders at different J_2 s. The “N/A” symbol means that the particular state can not be stabilized on that cylinder.

	$J_2 = 0.40$		$J_2 = 0.45$		$J_2 = 0.50$	
	Dimer	Collinear	Dimer	Collinear	Dimer	Collinear
XC8-0	-0.3007	-0.2981	-0.3112	-0.3078	-0.3229	-0.3189
XC10-0	N/A	-0.2981	N/A	-0.3077	N/A	-0.3188
XC12-0	-0.2985	-0.2978	-0.3083	-0.3076	-0.3196	-0.3188
YC4-0	-0.2982	N/A	N/A	-0.3078	N/A	-0.3189
YC6-0	-0.2978	-0.2978	N/A	-0.3070	N/A	-0.3189

In this table, we can see that the collinear states on these cylinders have relatively small finite size effects at fixed J_2 s. The collinear states can be stabilized on all the cylinders at different J_2 s, while the dimer state can be stabilized on XC8-0 and XC12-0 cylinders, where they are the real ground states. On YC cylinders, dimer states can only be obtained for small J_2 . The other tendency is that the energy difference between dimer and collinear state decreases as the cylinder becomes wider. At $J_2 = 0.5$, the dimer state is 1.2% lower than the collinear state on the XC8-0 cylinder, as compared to 0.25% lower on the XC12 cylinders. It may be possible that the ground state is the collinear state in the 2D limit for larger J_2 s.

Another interesting feature is that the diagonal dimer state is the ground state on all the cylinders for J_2 close to the second phase transition point ($J_2 = 0.37$). Therefore, we suspect that there might be a small phase region for $0.36 < J_2 < 0.4$ where the ground state is the dimer state. At larger J_2 s, the collinear state is more likely to be the ground state. In Ref. 39, the authors found that the energy difference between the VMC collinear state and small size exact diagonalization has a relatively large error of about 2.5% near the second phase transition point $J_2 = 0.35$ and a constant error of about 2% at $J_2 > 0.4$. This means that the variational wavefunction for the collinear state still doesn't quite capture the properties of the ground state (the dimer state) near $J_2 = 0.35$.

Series expansions find that the dimer state is marginally lower than the collinear state at $J_2 = 0.4$, while the collinear state is slightly lower at $J_2 = 0.5$. Therefore at large J_2 , there will be another phase transition point between the dimer and

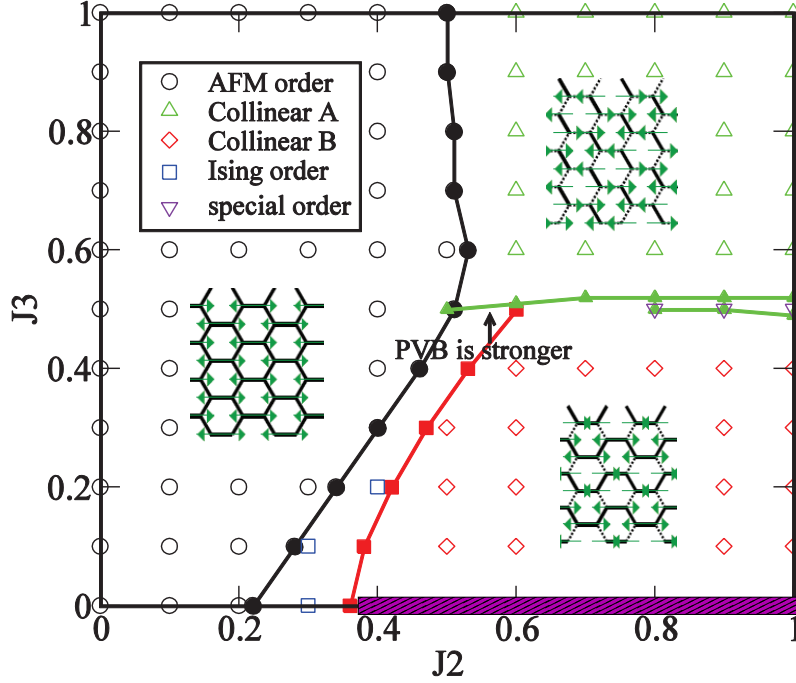


Fig. 8. The phase diagram with $J_1 - J_2 - J_3$ XY interactions on the honeycomb lattice. AFM and two types of collinear orders have moments in the xy plane. The Ising moments are along the z direction. Each symbol represents the state calculated with fixed J_2 and J_3 . The solid lines are the approximate phase transition points from J_2 or J_3 variation calculations on a single cylinder. The insets show what the three main phases (AFM and collinear A/B phase) look like, with solid bond indicating that nearest neighbor $\langle S_i \cdot S_j \rangle$ is negative and dashed bond for positive. See the text for details on the special order phase. The purple pattern at the $J_3 = 0$ axis with $J_2 > 0.36$ is the region where the ground state is the dimer state on the XC8-0 cylinder. We do not understand how this phase is connected with the collinear B phase.

collinear state.³⁶ The coupled cluster method for the dimer response in the collinear state finds a strong competition between collinear and dimer states at $0.355(5) < J_2 < 0.52(3)$. At $J_2 > 0.52(3)$, the collinear state is more favorable.³⁷ Although the dimer state first found by DMRG was not predicted from either small size exact diagonalization or VMC calculations,^{28,39} all these numerical methods both agree that there is a close competition between dimer and collinear state closer to $J_2 = 0.36$, albeit it is delicate to determine the transition between dimer and collinear state.

3. Phase diagram of $J_1 - J_2 - J_3$ XY model on the XC8-0 cylinder

Searching for possible SL states in the honeycomb lattice with only XY interactions, we added third-neighbor interactions (J_3 terms) to the system to scan the

whole phase diagram in Fig. 8. Since adding another parameter J_3 greatly increase the numerical effort, we only performed DMRG calculations on XC8-0 cylinders. We first calculated the ground states on a set of XC8-0 cylinders with J_2 and J_3 starting at $J_2 = 0$ and $J_3 = 0$, then increase each parameter separately by 0.1 on each cylinder. The couplings were constant along the length. By applying pinning magnetic fields along the x -direction on the cylinder edges, we characterized each specific state. The phase transition lines are determined by calculating a cylinder with J_2 or J_3 varying along the length while fixing the other parameter as in Fig. 1(a).

J_3 interaction actually favors Neel order. Therefore, we expect that the phase transition point between Neel and Ising order should move to higher J_2 with increasing J_3 . This is confirmed on the bottom solid black line on Fig. 8 for $J_3 < 0.5$. Then with $J_3 > 0.5$, there is a phase transition between Neel and collinear A ordered phase. Collinear A phase only have AFM spins along one particular diagonal direction. The phase transition between them is located roughly at $J_2 = 0.5$ and $J_3 > 0.5$. This phase boundary matches the classical phase diagram for Neel and collinear A phase.

The red solid line is the phase transition between Ising and a different collinear B phase. The intermediate phase region (between solid black and red line) has very robust Ising order at small J_3 . But Ising order parameter decreases as J_3 increasing. At around $J_2 = 0.6$ and $J_3 = 0.5$, valence bond order is much stronger. Therefore, we suspect that there might be a phase transition between Ising and valence bond order for the intermediate phase regime. We will not focus on this issue in the paper.

The green line is the phase boundary between collinear A and B phase. At J_2 close to 1, we find that there exists a small region at $0.49 < J_3 < 0.52$ and $0.8 < J_2 < 1.0$, which we call the special order phase. This phase has very weak nearest neighbor bonds, but with strong bonds along the vertical second-neighbor and horizontal third-neighbor directions forming a rectangular lattice. This pattern breaks the honeycomb lattice six fold rotational symmetry, and thus it is also not a spin liquid state. It would be interesting to check if this phase is presented on the wider cylinders.

Note that the collinear B phase is different from the collinear phase in Fig. 6(d) at $J_3 = 0$. At $J_3 = 0$, the metastable collinear phase has AFM correlated zigzag chains with FM correlations between them. But with a little J_3 interaction added to the system, the ground state forms a different type of collinear phase with AFM correlated chains along the armchair direction of the hexagon lattice. It's hard for us to determine the phase transition between these two collinear states specifically. But we can understand this from the following classical picture, instead of including classical spin spiral states.

The classical energy for a Neel state E_N , for a collinear state with AFM correlation in zigzag chains (collinear Z state in Fig. 6d) E_z , for a collinear A state E_A

and for a collinear B states E_B are as follows:

$$\begin{aligned} E_N &= -\frac{3}{8} (J_1 - 2J_2 + J_3) \\ E_z &= -\frac{1}{8} (J_1 + 2J_2 - 3J_3) \\ E_A &= \frac{1}{8} (J_1 - 2J_2 - 3J_3) \\ E_B &= -\frac{1}{8} (J_1 + 2J_2 - J_3) \end{aligned} \quad (3)$$

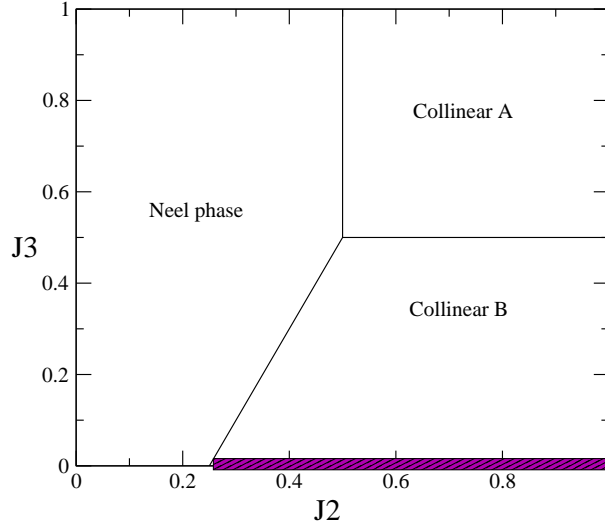


Fig. 9. The classical phase diagram for the $J_1 - J_2 - J_3$ XY model, where we only consider several classical states -Neel, collinear Z, A and B states. Only at $J_3 = 0$ and $J_2 > 0.25$ (the purple region), collinear Z and B states have the same energy.

For $J_3 = 0$, two classical collinear states E_z and E_B have exactly the same energy. However with $J_3 > 0$, only the classical collinear B state has lower energy. These two collinear states in the quantum limit have similar properties as classical states. Thus only the collinear B state is possible for $J_3 > 0$ in the quantum limit. For $0 < J_3 < 0.5$, the classical ground state has a transition from a Neel to a collinear B state, with phase transition changing from $J_2 = 0.25$ at $J_3 = 0$ to $J_2 = 0.5$ at $J_3 = 0.5$. For $J_3 > 0.5$, the classical ground state has a phase transition from a Neel to a collinear A state. The transition between collinear A to collinear B state is located at $0.5 < J_2 < 1$ with $J_3 = 0.5$. These classical states phase diagram is shown in Fig. 9.

Comparing these classical phase diagram with the quantum phase diagram in Fig. 8, the Neel, collinear A and collinear B states appear in almost the same place in phase diagram, except the phase boundary varies slightly. The other difference is that there is a intermediate phase between the Neel and the collinear B state in the

quantum limit. At $J_3 = 0$, the large J_2 phase (purple region) is the dimer state for quantum case on the XC8-0 cylinder. In summary, even with an extra parameter J_3 included, we still could not find any trace of a spin liquid state on the honeycomb lattice with only XY interaction.

4. The transition between $J_1 - J_2$ XY and Heisenberg model at $J_2 = 0.3$

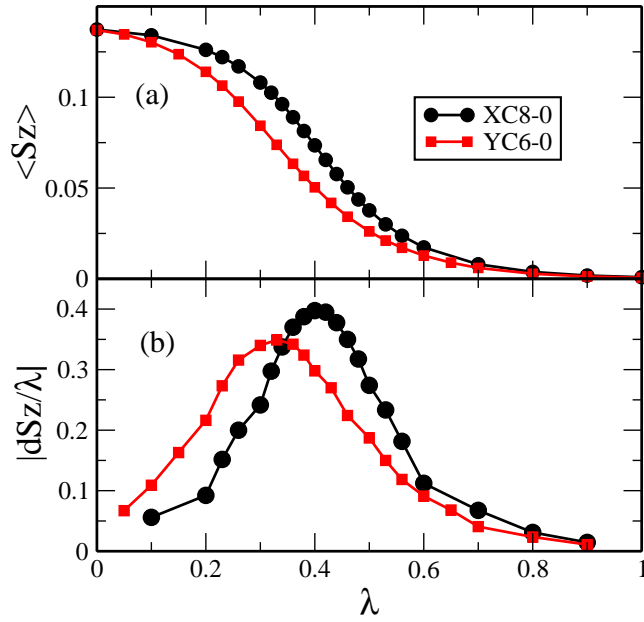


Fig. 10. (a) The magnetization $\langle S_z \rangle$ in the cylinder center for XC8-0 and YC6-0 cylinders versus the S_z coupling λ (see Eq. 4) for $J_2 = 0.3$. (b) The first order derivative of $\langle S_z \rangle$ versus coupling λ . The peak indicates the possible phase transition between $J_1 - J_2$ XY model and $J_1 - J_2$ Heisenberg model for $J_2 = 0.3$ at around $0.35 \sim 0.4$.

Finally in this section, we briefly discuss the effect when the S_z interaction is included. The Hamiltonian we considered is:

$$\begin{aligned}
 H = & \sum_{\langle i,j \rangle} J_1 (S_i^x S_j^x + S_i^y S_j^y + \lambda S_i^z S_j^z) \\
 & + \sum_{\langle\langle i,j \rangle\rangle} J_2 (S_i^x S_j^x + S_i^y S_j^y + \lambda S_i^z S_j^z).
 \end{aligned} \tag{4}$$

For $\lambda = 0$, this Hamiltonian is exactly as Eq. (1), it is just a pure $J_1 - J_2$ XY model. For $\lambda = 1$, the Hamiltonian is the $J_1 - J_2$ Heisenberg model.

The $J_1 - J_2$ Heisenberg model has been studied extensively in the literature for the past few years.^{40,41,42,43,44,45,46,47,48,49} Like the XY model case, the Heisenberg model also has an intermediate phase. All the references agree that this intermediate phase has no magnetic order. Initially there has been controversy about the existence of SL or plaquette valence bond (PVB) order for this phase. But recent DMRG calculations found that this intermediate phase has long range PVB order, although there might be a very narrow parameter regime near the first critical point where the SL phase is possible. DMRG calculation from Ref. 34 found the intermediate phase regime between $0.26 < J_2 < 0.36$. Ref. 50 measured the two phase transition points located at 0.22 and 0.35. Ref. 51 pointed out the PVB order is between 0.25 and 0.35, with a narrow regime ($0.22 < J_2 < 0.25$) where a SL state is possible. However the SL regime might be a finite size effect, which may disappear on larger systems.

Therefore when tuning the parameter λ from 0 to 1 inside the intermediate phase, there must be a phase transition between Ising and PVB order, i.e. the $S_z S_z$ interactions terms will disfavor the Ising order. It would be interesting to see where the phase transition is. Next we will focus on this transition only at $J_2 = 0.3$ for the intermediate phase.

In Fig. 10, we present the magnetization calculated on XC8-0 and YC6-0 cylinders with Hamiltonian in Eq. 4 for various λ at $J_2 = 0.3$. We also apply a pinning magnetic field h_z in both the cylinder edges to favor only one kind of Ising pattern. For a pure XY model with $\lambda = 0$, magnetization in the cylinder center is maximum. However, with increasing λ , magnetization decreases faster at $\lambda \sim 0.4$ to almost zero at the Heisenberg limit with $\lambda = 1$. The peak of the first order derivative of $\langle S_z \rangle$ can roughly determine where the magnetization changes fastest. The peak is located at 0.40 for the XC8-0 cylinder and 0.35 for the YC6-0 cylinder. Thus there may be a possible phase transition around $0.35 \sim 0.40$. It would be useful to perform similar calculations on wider cylinders like XC10-0 and XC12-0 in the future. If the derivative curve becomes sharper and position of the peak does not change too much, we can determine the phase transition points confidently in the thermodynamic limit.

A recent paper⁵² by Li *et. al.* studied the same Hamiltonian as Eq. 4 with the coupled cluster method for the whole phase diagram in the parameter $J_2 - \lambda$ space. They found that as increasing $S_z S_z$ coupling λ , the Ising order phase changes to a possible SL state for $0.21 < J_2 < 0.28(2)$ and PVB order for $0.28(2) < J_2 < 0.38$. At $J_2 = 0.3$, they found the transition at $\lambda = 0.65$, much larger than $\lambda = 0.35 \sim 0.40$ from the DMRG calculations. Meanwhile the boundary between SL and PVB order state has much larger uncertainty. At the Heisenberg limit, they suggested a larger regime of possible SL states ($0.21 < J_2 < 0.28(2)$), much larger than the regime claimed by DMRG⁵¹ ($0.22 < J_2 < 0.25$). Therefore, it is still an unsolved issue for the Heisenberg limit, whether there would be a possible SL phase near the first phase transition point. Perhaps future numerical studies from the tensor network method, which works directly toward the thermodynamic limit, such as projected

entangled pair states (PEPS)^{53,54,55} and multi-scale entanglement renormalization ansatz (MERA)^{56,57} would provide some new insights into the possible existence of the SL phase in the phase diagram.

5. Summary

In summary, we have reviewed the study of $J_1 - J_2$ antiferromagnetic spin-1/2 XY model on the honeycomb lattice. Instead of a spin-liquid ground state in the intermediate phase regime for $0.22 < J_2/J_1 < 0.36$, there exists an Ising ordered phase with a staggered magnetization along the z direction that does not show any strong finite size effects. Its ground state energy is much lower than proposed spin-liquid states with a vanishing topological entanglement entropy. Thinking about this in terms of the spin model, it is somewhat puzzling to understand why this phase appears, since there are no $S_i^z S_j^z$ interaction terms in the spin Hamiltonian. It seems like only the XY model honeycomb lattice with low coordination number has this exotic phase. We do not find any Ising ordered phase of the same model on the square, kagome or triangular lattice. Describing the system instead as hard-core bosons with frustrated hopping, this Ising phase is then a Mott insulator with one boson per two-site unit cell, and the Ising order is then CDW order that breaks the Z_2 sublattice symmetry of the unit cell. The on-site hard-core interaction must induce a first-neighbor repulsion that stabilizes this CDW order. Thus, although this model unfortunately does not appear to exhibit a spin-liquid ground state, it exhibits this somewhat surprising CDW Z_2 ordered phase. Although the third neighbor J_3 XY interaction or the $S_i^z S_j^z$ interaction disfavor the Ising ordered phase, the system either evolves into a PVB ordered state or a magnetic ordered state, instead of a SL state.

Acknowledgments

We would like to thank David Huse, Sasha Chernyshev, Leonid Glazman, Andreas Laeuchli, Sid Parameswaran, Rajiv Singh, Raymond Bishop, Marcos Rigol, Victor Galitski, Tigran Sedrakyan, Juan Carrasquilla, Hongcheng Jiang, Leon Balents, Miles Stoudenmire, and Simeng Yan for many helpful discussions. This work was supported by NSF Grant No. DMR-1161348 (Z.Z., S.R.W.).

References

1. P. W. Anderson, *Mater. Res. Bull.* **8**, 153, (1973).
2. D. A. Huse and U. Elser, *Phys. Rev. Lett.* **60**, 253 (1988).
3. L. Balents, *Nature (London)* **464**, 199 (2010) and references therein.
4. D. S. Rokhsar and S. A. Kivelson, *Phys. Rev. Lett.* **61**, 2376 (1988)
5. R. Moessner and S. L. Sondhi, *Phys. Rev. Lett.* **86**, 1881 (2001)
6. A. Y. Kitaev, *Ann. Phys.* **303**, 2 (2003)
7. M. A. Levin and X. G. Wen, *Phys. Rev. B* **71**, 045110 (2005)
8. S. Yan, D. A. Huse, and S. R. White, *Science* **332**, 1173 (2011).

9. A. Kitaev and J. Preskill, Phys. Rev. Lett. **96**, 110404 (2006).
10. M. Levin and X. G. Wen, Phys. Rev. Lett. **96**, 110405 (2006).
11. J. S. Helton, K. Matan, M. P. Shores, E. A. Nytko, B. M. Bartlett, Y. Yoshida, Y. Takano, A. Suslov, Y. Qiu, J.-H. Chung, D. G. Nocera, and Y. S. Lee, Phys. Rev. Lett. **98**, 107204 (2007).
12. M. A. de Vries, K. V. Kamenev, W. A. Kockelmann, J. Sanchez-Benitez, and A. Harrison, Phys. Rev. Lett. **100**, 157205 (2008).
13. J. S. Helton, K. Matan, M. P. Shores, E. A. Nytko, B. M. Bartlett, Y. Qiu, D. G. Nocera, and Y. S. Lee, Phys. Rev. Lett. **104**, 147201 (2010).
14. T. H. Han, J. S. Helton, S. Chu, A. Prodi, D. K. Singh, C. Mazzoli, P. Muller, D. G. Nocera, and Y. S. Lee, Phys. Rev. B **83**, 100402(R) (2011).
15. T. H. Han, J. S. Helton, S. Chu, D. G. Nocera, J. A. R.-Rivera, C. Broholm, and Y. S. Lee, Nature (London) **492**, 406 (2012).
16. S. Depenbrock, I. P. McCulloch, and U. Schollwock, Phys. Rev. Lett. **109**, 067201 (2012).
17. H. C. Jiang, Z. H. Wang, and L. Balents, Nat. Phys. **8**, 902 (2012).
18. S. R. White, Phys. Rev. Lett. **69**, 2863 (1992).
19. S. R. White, Phys. Rev. B **48**, 10345 (1993).
20. E. M. Stoudenmire and S. R. White, Annu. Rev. Condens. Matter Phys. **3**, 111 (2012).
21. Z. Y. Meng, T. C. Lang, S. Wessel, F. F. Assaad and A. Muramatsu, Nature **464**, 847, (2010).
22. H. Jiang, H. Yao and L. Balents, Phys. Rev. B **86**, 024424, (2012).
23. L. Wang, Z.-C. Gu, X.-G. Wen and F. Verstraete, arXiv:1112.3331, (unpublished).
24. Sandro Sorella, Yuichi Otsuka, Seiji Yunoki, Scientific Reports **2**, 992, (2012).
25. A. W. Sandvik, Phys. Rev. B **85**, 134407, (2012).
26. F. F. Assaad and I. F. Herbut, Phys. Rev. X **3**, 031010 (2013).
27. S.-S. Gong, W. Zhu, D. N. Sheng, O. I. Motrunich, M. P. A. Fisher, Phys. Rev. Lett. **113**, 027201 (2014).
28. C. N. Varney, K. Sun, V. Galitski, and M. Rigol, Phys. Rev. Lett. **107**, 077201 (2011).
29. D. N. Sheng, O. I. Motrunich, and M. P. A. Fisher, Phys. Rev. B **79**, 205112 (2009).
30. M. S. Block, D. N. Sheng, O. I. Motrunich, and M. P. A. Fisher, Phys. Rev. Lett. **106**, 157202 (2011).
31. I. Kimchi, S. A. Parameswaran, A. M. Turner, F. Wang and A. Vishwanath, Proc. Natl. Acad. Sci. U.S.A. **110**, 16378 (2013).
32. T. A. Sedrakyan, L. I. Glazman, and A. Kamenev, Phys. Rev. B **89**, 201112 (2014).
33. Z. Zhu, D. A. Huse, and S. R. White, Phys. Rev. Lett. **111**, 257201 (2013).
34. Z. Zhu, D. A. Huse, and S. R. White, Phys. Rev. Lett. **110**, 127205 (2013).
35. A. Di Ciolo, J. Carrasquilla, F. Becca, M. Rigol, and V. Galitski, Phys. Rev. B **89**, 094413 (2014).
36. J. Oitmaa, AND R. R. P. Singh, Phys. Rev. B **89**, 104423 (2014).
37. R. F. Bishop, P. H. Y. Li, and C. E. Campbell, Phys. Rev. B **89**, 214413 (2014).
38. J. Eisert, M. Cramer, and M. B. Plenio, Rev. Mod. Phys. **82**, 277 (2010).
39. J. Carrasquilla, A. Di Ciolo, F. Becca, V. Galitski, and M. Rigol, Phys. Rev. B **88**, 241109 (2013).
40. A. F. Albuquerque, D. Schwandt, B. Hetényi, S. Capponi, M. Mambrini and A. M. Läuchli, Phys. Rev. B **84**, 024406, (2011).
41. H. Mosadeq, F. Shahbazi, and S. A. Jafari, J. Phys.: Condens. Matter **23**, 226006, (2011).
42. D. J. J. Farnell, R. F. Bishop, P. H. Y. Li, J. Richter and C. E. Campbell, Phys. Rev. B **84**, 012403, (2011).

43. J. Oitmaa, and R. R. P. Singh, Phys. Rev. B **84**, 094424, (2011).
44. J. Reuther, D. A. Abanin, and R. Thomale, Phys. Rev. B **84**, 014417, (2011).
45. J. B. Fouet, P. Sindzingre, C. Lhuillier, Eur. Phys. J. B. **20**, 241, (2001).
46. A. Mulder, R. Ganesh, L. Capriotti, and A. Paramekanti, Phys. Rev. B **81**, 214419, (2010).
47. D. C. Cabra, C. A. Lamas, and H. D. Rosales, Mod. Phys. Lett. B **25**, 891, (2011).
48. F. Mezzacapo and M. Boninsegni, Phys. Rev. B **85**, 060402, (2012).
49. B. K. Clark, D. A. Abanin, and S. L. Sondhi, Phys. Rev. Lett. **332**, 1173, (2011).
50. R. Ganesh, J. van den Brink, and S. Nishimoto, Phys. Rev. Lett. **110** 127203, (2013).
51. S.-S. Gong, D. N. Sheng, O. I. Motrunich, and M. P. A. Fisher, Phys. Rev. B **88** 165138, (2013).
52. P. H. Y. Li, R. F. Bishop, and C. E. Campbell, Phys. Rev. B **89** 220408, (2014).
53. F. Verstraete, V. Murg and J. Cirac, Adv. Phys. **57** 143, (2008).
54. J. Jordan, R. Orus, G. Vidal, F. Verstraete and J. Cirac, Phys. Rev. Lett. **101** 250602, (2008).
55. R. Orus and G. Vidal, Phys. Rev. B **80** 094403, (2009).
56. G. Vidal, Phys. Rev. Lett. **99** 220405, (2007).
57. G. Evenbly and G. Vidal, Phys. Rev. B **79** 144108, (2009).